Supporting Information

# Crystal Structure, Stability and Li Superionic Conductivity of Pyrochlore-Type Solid Electrolyte $Li_{2-x}La_{(1+x)/3}Nb_2O_6F$: A First-Principles Calculation Study

Randy Jalem,[1,*] Kazunori Takada,[1] Hitoshi Onodera[2], and Shuhei Yoshida[2]

[1]Center for Green Research on Energy and Environmental Materials (GREEN), National Institute for Materials Science (NIMS), 1-1 Namiki, Tsukuba, Ibaraki 305-0044, Japan

[2]Environment Neutral System Development Division, DENSO CORPORATION, 1 Yoshiike, Kusagi, Agui-cho, Chita-gun, Aichi 470-2298, Japan

Email: JALEM.Randy@nims.go.jp

*Material synthesis*

The $Li_{1.25}La_{0.58}Nb_2O_6F$ (LLNOF) solid electrolyte was prepared using the following synthesis conditions. $Li_2CO_3$, $La_2O_3$ and $Nb_2O_5$ reactant powders in stoichiometric ratio were calcined at 773 K and then heated at 1473 K for 6 hours to synthesize the precursor $Li_{0.5}La_{0.5}Nb_2O_6$. Next, the synthesized $Li_{0.5}La_{0.5}Nb_2O_6$ was mixed with $LaF_3$ and LiF. Here, 91%-excess LiF was added. The mixture was then heated at 1273 K for 6 hours to synthesize the target LLNOF powder.

*Cyclic voltammetry measurement*

The LLNOF electrolyte, acetylene black (AB) (conductive additive), and polyvinylidene fluoride (PVDF) (binder) were weighed in a mass ratio of 70:10:20 and then mixed with N-methyl-2-pyrrolidone (NMP) to form a paste. The paste was applied onto a copper foil and dried to make an electrode. The cyclic voltammetry evaluation was conducted using a 2032-type coin cell assembled with a Li anode. The electrolyte used was a solution of 1M $LiPF_6$ dissolved in a mixture of ethylene carbonate (EC) and dimethyl carbonate (DEC) in a volume ratio of 1:1. The coin cells were assembled in an Ar atmosphere inside a glove box. Cyclic voltammetry measurements were performed using a potentiostat/galvanostat device, with a scan voltage range of 0.02 V to 3V and a scan rate of 10 mV/s at 25°C.

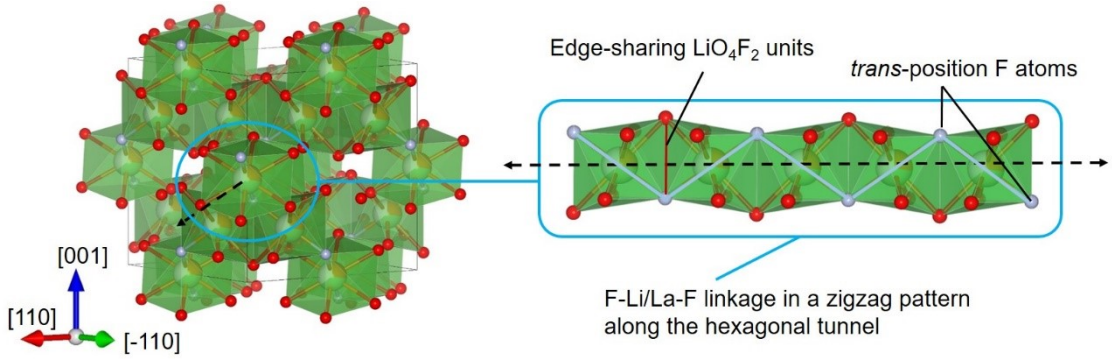


Figure S1. Visualization of the local structure of pyrochlore-type $Li_{2-x}La_{(1+x)/3}Nb_2O_6F$ (LLNOF) showing the F-Li/La-F linkage in a zigzag pattern along the characteristic hexagonal tunnel. The octahedral $NbO_6$ units are not displayed for clarity.

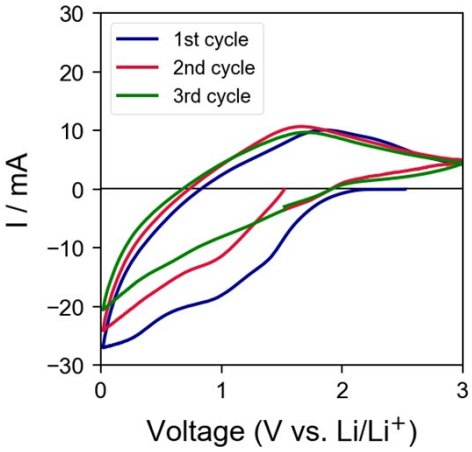


Figure S2. Cyclic voltammetry curves for the 1st, 2nd, and 3rd cycle of cell with LLNOF solid electrolyte.

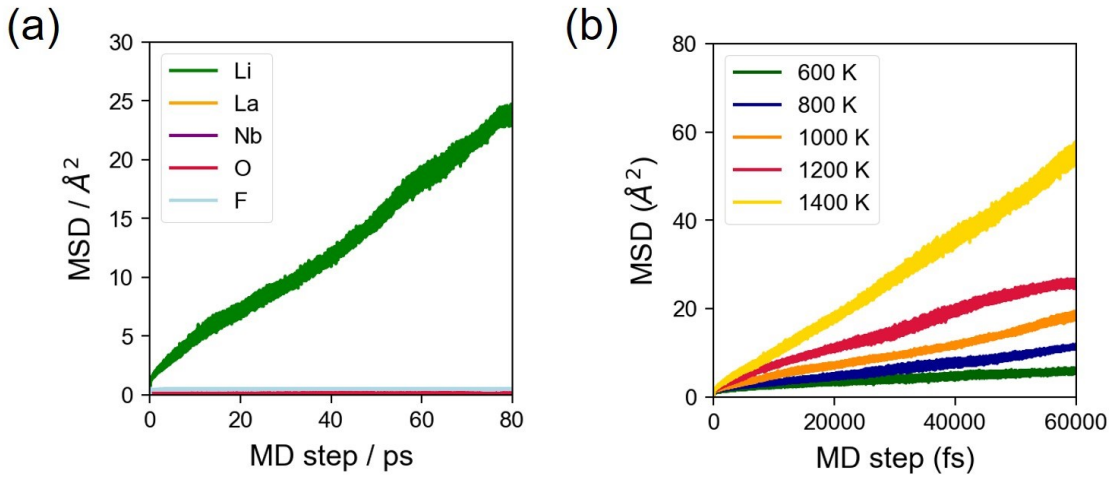


Figure S3. Mean squared displacement ($MSD$) plots for (a) each atom types at 1000 K and (b) Li atoms in pyrochlore-type $Li_{1.3125}La_{0.5625}Nb_2O_6F$ with the L1 structure (LLNOF-L1) from by NVT-AIMD calculations.

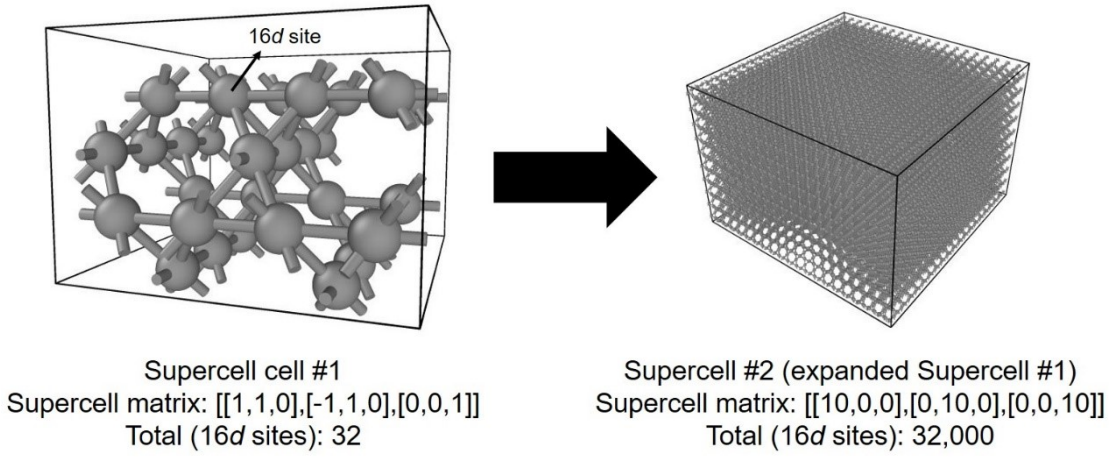


Figure S4. Supercell operation of the 16*d*-site cation sublattice in the $Li_{2-x}La_{(1+x)/3}Nb_2O_6F$ crystal structure for use in the calculation of $Li^+$ percolation threshold.

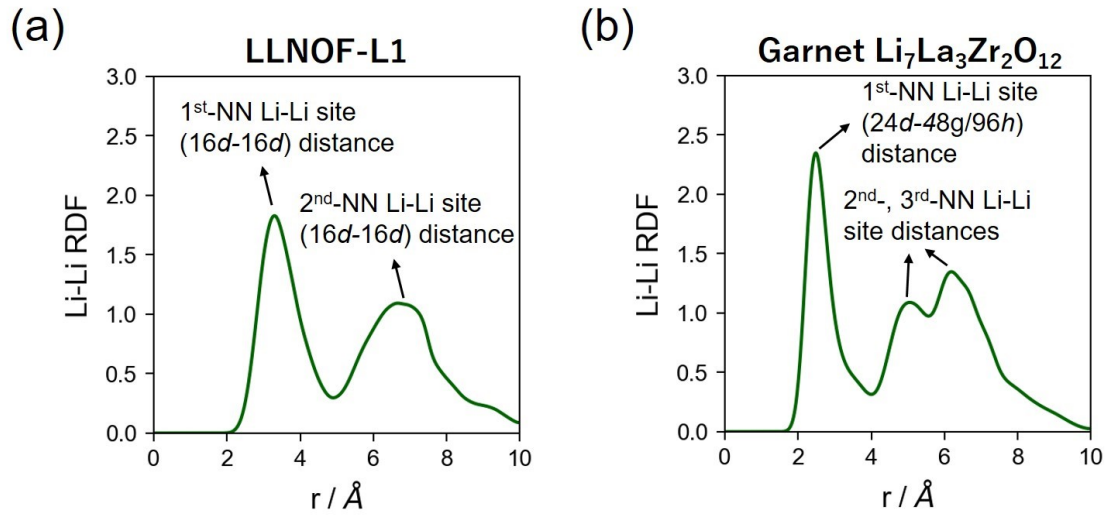


Figure S5. Li-Li radial distribution function (RDF) profiles derived from 1000-K NVT AIMD calculations for (a) pyrochlore-type $Li_{1.3125}La_{0.5625}Nb_2O_6F$ with the L1 structure (LLNOF-L1) and (b) garnet-type cubic $Li_7La_3Zr_2O_{12}$.

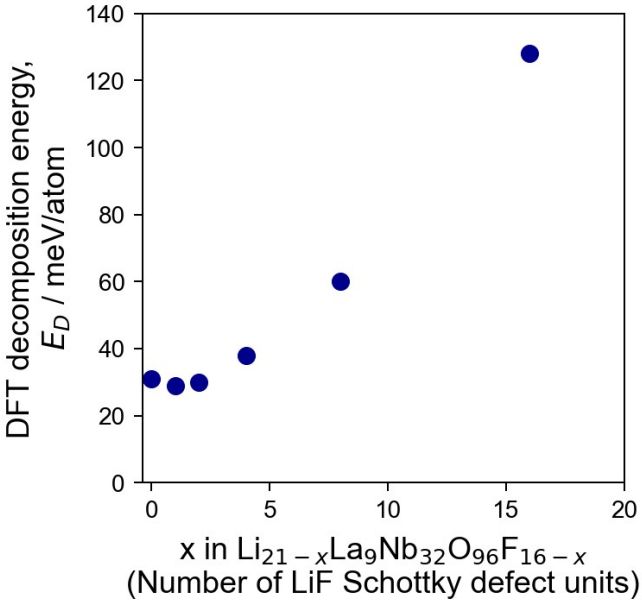


Figure S6. Plot for DFT decomposition energy as a function of the number of LiF Schottky defect units. The initial reference structure was based on $Li_{1.3125}La_{0.5625}Nb_2O_6F$ composition (L1 structure, supercell formula is $Li_{21}La_9Nb_{32}O_{96}F_{16}$ which is for x = 0).

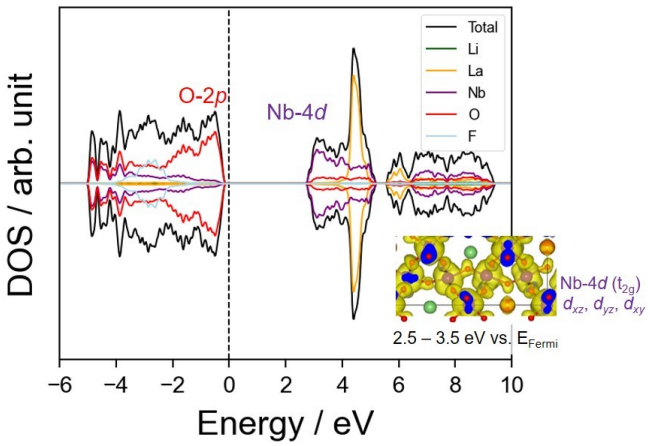


Figure S7. DFT-GGA electronic density of states (DOS) of pyrochlore-type $Li_{1.3125}La_{0.5625}Nb_2O_6F$ (LLNOF-L1 structure). The Fermi energy is referenced as zero in the horizontal axis.

Table S1. Crystal structure coordinate data of LLNOF by XRD Rietveld analysis, as reported in Ref. 12. Space group: $Fd\bar{3}m$ (cubic), lattice parameter $a$: 1.0445(1) nm, cell volume: 1.1396(1) $nm^3$.

| Atom | Site | Occupancy (g) | Coordinates | | |
|---|---|---|---|---|---|
| | | | x | y | z |
| La | 16d | 0.2771(6) | 1/2 | 1/2 | 1.2 |
| Li | 16d | 0.365(15) | x(La) | y(La) | z(La) |
| Nb | 16c | 1.0 | 0 | 0 | 0 |
| O | 48f | 1.0 | 0.3151(2) | 1/8 | 1/8 |
| F | 8b | 0.989(8) | 3/8 | 3/8 | 3/8 |

Table S2. Summary of DFT-predicted decomposition reactions related to the voltage stability window of pyrochlore-type $Li_{1.3125}La_{0.5625}Nb_2O_6F$ with the L1 structure (LLNOF-L1).

| Voltage / V vs. $Li/Li^+$ | Decomposition reaction |
|---|---|
| 0 – 0.54 | $Li_{21}La_9Nb_{32}(O_6F)_{16}$ + 160 Li → 4.5 $La_2O_3$ + 16 LiF + 82.5 $Li_2O$ + 32 Nb |
| 0.54 – 0.62 | $Li_{21}La_9Nb_{32}(O_6F)_{16}$ + 64 Li → 4.5 $La_2O_3$ + 32 $LiNbO_2$ + 16 LiF + 18.5 $Li_2O$ |
| 0.62 – 0.96 | $Li_{21}La_9Nb_{32}(O_6F)_{16}$ + 49.2 Li → 3.7 $Li_8Nb_2O_9$ + 4.5 $La_2O_3$ + 24.6 $LiNbO_2$ + 16 LiF |
| 0.96 – 0.99 | $Li_{21}La_9Nb_{32}(O_6F)_{16}$ + 45.5 Li → 4.5 $La_2O_3$ + 22.75 $LiNbO_2$ + 9.25 $Li_3NbO_4$ + 16 LiF |
| 0.99 – 1.33 | $Li_{21}La_9Nb_{32}(O_6F)_{16}$ + 41 Li → 20.5 $LiNbO_2$ + 11.5 $Li_3NbO_4$ + 7 LiF + 9 LaOF |
| 1.33 – 1.74 | $Li_{21}La_9Nb_{32}(O_6F)_{16}$ + 32 Li → 16 $LiNbO_2$ + 9 $LaNbO_4$ + 7 $Li_3NbO_4$ + 16 LiF |
| 1.74 – 1.92 | $Li_{21}La_9Nb_{32}(O_6F)_{16}$ + 18 Li → 14 $LiNbO_3$ + 9 $LiNbO_2$ + 9 $LaNbO_4$ + 16 LiF |
| 1.92 – 2.35 | $Li_{21}La_9Nb_{32}(O_6F)_{16}$ + 2.571 Li → 7.571 $LiNbO_3$ + 1.286 $Nb_{12}O_{29}$ + 9 $LaNbO_4$ + 16 LiF |
| 2.35 – 2.49 | $Li_{21}La_9Nb_{32}(O_6F)_{16}$ + 0.8889 Li → 5.889 $LiNb_3O_8$ + 0.4444 $Nb_{12}O_{29}$ + 9 $LaNbO_4$ + 16 LiF |
| 2.49 – 3.92 | $Li_{21}La_9Nb_{32}(O_6F)_{16}$ → 5 $LiNb_3O_8$ + 9 $LaNbO_4$ + 4 $Nb_2O_5$ + 16 LiF |
| 3.92 – 3.93 | $Li_{21}La_9Nb_{32}(O_6F)_{16}$ → 9 $LaNbO_4$ + 11.5 $Nb_2O_5$ + 16 LiF + 1.25 $O_2$ + 5 Li |
| 3.93 – | $Li_{21}La_9Nb_{32}(O_6F)_{16}$ → 3.667 $LaNbO_4$ + 14.17 $Nb_2O_5$ + 5.333 $LaF_3$ + 5.25 $O_2$ + 21 Li |

Table S3. Summary of DFT-predicted decomposition reactions related to the voltage stability window of $Li_3Nb_3O_8$ which is one of the decomposition phases of pyrochlore-type $Li_{1.3125}La_{0.5625}Nb_2O_6F$ with the L1 structure (LLNOF-L1).

| Voltage / V vs. $Li/Li^+$ | Decomposition reaction |
|---|---|
| 0 – 0.54 | 4 $LiNb_3O_8$ + 60 Li → 32 $Li_2O$ + 12 Nb |
| 0.54 – 0.62 | 4 $LiNb_3O_8$ + 24 Li → 12 $LiNbO_2$ + 8 $Li_2O$ |
| 0.62 – 0.96 | 4 $LiNb_3O_8$ + 17.6 Li → 1.6 $Li_8Nb_2O_9$ + 8.8 $LiNbO_2$ |
| 0.96 – 1.74 | 4 $LiNb_3O_8$ + 16 Li → 4 $Li_3NbO_4$ + 8 $LiNbO_2$ |
| 1.74 – 1.92 | 4 $LiNb_3O_8$ + 8 Li → 8 $LiNbO_3$ + 4 $LiNbO_2$ |

| | |
|---|---|
| 1.92 – 2.35 | 4 $LiNb_3O_8$ + 1.143 Li → 5.143 $LiNbO_3$ + 0.5714 $Nb_{12}O_{29}$ |
| 2.35 – 3.92 | 4 $LiNb_3O_8$ → 4 $LiNb_3O_8$ |
| 3.92 – | 4 $LiNb_3O_8$ → 6 $Nb_2O_5$ + $O_2$ + 4 Li |

Table S4. Summary of DFT-predicted decomposition reactions related to the voltage stability window of LiF which is one of the decomposition phases of pyrochlore-type $Li_{1.3125}La_{0.5625}Nb_2O_6F$ with the L1 structure (LLNOF-L1).

| Voltage / V vs. $Li/Li^+$ | Decomposition reaction |
|---|---|
| 0 – 6.36 | LiF → LiF |
| 6.36 – | LiF → 0.5 $F_2$ + Li |

Table S5. Summary of DFT-predicted decomposition reactions related to the voltage stability window of $LaNbO_4$ which is one of the decomposition phases of pyrochlore-type $Li_{1.3125}La_{0.5625}Nb_2O_6F$ with the L1 structure (LLNOF-L1).

| Voltage / V vs. $Li/Li^+$ | Decomposition reaction |
|---|---|
| 0 – 0.54 | 2 $LaNbO_4$ + 10 Li → 5 $Li_2O$ + $La_2O_3$ + 2 Nb |
| 0.54 – 0.62 | 2 $LaNbO_4$ + 4 Li → 2 $LiNbO_2$ + $Li_2O$ + $La_2O_3$ |
| 0.62 – 0.96 | 2 $LaNbO_4$ + 3.2 Li → 1.6 $LiNbO_2$ + 0.2 $Li_8Nb_2O_9$ + $La_2O_3$ |
| 0.96 – 1.06 | 2 $LaNbO_4$ + 3 Li → 0.5 $Li_3NbO_4$ + 1.5 $LiNbO_2$ + $La_2O_3$ |
| 1.06 – 1.30 | 2 $LaNbO_4$ + 2 Li → 0.3333 $Li_3NbO_4$ + 0.6667 $La_3NbO_7$ + $LiNbO_2$ |
| 1.30 – | 2 $LaNbO_4$ → 2 $LaNbO_4$ |

Table S6. Summary of DFT-predicted decomposition reactions related to the voltage stability window of $Nb_2O_5$ which is one of the decomposition phases of pyrochlore-type $Li_{1.3125}La_{0.5625}Nb_2O_6F$ with the L1 structure (LLNOF-L1).

| Voltage / V vs. $Li/Li^+$ | Decomposition reaction |
|---|---|
| 0 – 0.54 | 14 $Nb_2O_5$ + 140 Li → 70 $Li_2O$ + 28 Nb |
| 0.54 – 0.62 | 14 $Nb_2O_5$ + 56 Li → 28 $LiNbO_2$ + 14 $Li_2O$ |
| 0.62 – 0.96 | 14 $Nb_2O_5$ + 44.8 Li → 2.8 $Li_8Nb_2O_9$ + 22.4 $LiNbO_2$ |
| 0.96 – 1.74 | 14 $Nb_2O_5$ + 42 Li → 7 $Li_3NbO_4$ + 21 $LiNbO_2$ |
| 1.74 – 1.92 | 14 $Nb_2O_5$ + 28 Li → 14 $LiNbO_3$ + 14 $LiNbO_2$ |
| 1.92 – 2.35 | 14 $Nb_2O_5$ + 4 Li → 4 $LiNbO_3$ + 2 $Nb_{12}O_{29}$ |

| | |
|---|---|
| 2.35 – 2.49 | 14 $Nb_2O_5$ + 3.111 Li → 3.111 $LiNb_3O_8$ + 1.556 $Nb_{12}O_{29}$ |
| 2.49 – | 14 $Nb_2O_5$ → 14 $Nb_2O_5$ |

Table S7. Summary of DFT-predicted decomposition reactions related to the voltage stability window of garnet-type cubic $Li_7La_3Zr_2O_{12}$.

| Voltage / V vs. $Li/Li^+$ | Decomposition reaction |
|---|---|
| 0 – 0.04 | 4 $Li_7La_3Zr_2O_{12}$ + 28 Li → 2 $Zr_4O$ + 28 $Li_2O$ + 6 $La_2O_3$ |
| 0.04 – 0.05 | 4 $Li_7La_3Zr_2O_{12}$ + 26.67 Li → 2.667 $Zr_3O$ + 27.33 $Li_2O$ + 6 $La_2O_3$ |
| 0.05 – 2.90 | 4 $Li_7La_3Zr_2O_{12}$ → 4 $Li_6Zr_2O_7$ + 2 $Li_2O$ + 6 $La_2O_3$ |
| 2.90 – 3.16 | 4 $Li_7La_3Zr_2O_{12}$ → 4 $Li_6Zr_2O_7$ + $Li_2O_2$ + 6 $La_2O_3$ + 2 Li |
| 3.16 – 3.24 | 4 $Li_7La_3Zr_2O_{12}$ → 7 $Li_2O_2$ + 4 $La_2Zr_2O_7$ + 2 $La_2O_3$ + 14 Li |
| 3.24 – 3.72 | 4 $Li_7La_3Zr_2O_{12}$ → 1.75 $LiO_8$ + 4 $La_2Zr_2O_7$ + 2 $La_2O_3$ + 26.25 Li |
| 3.72 – | 4 $Li_7La_3Zr_2O_{12}$ → 4 $La_2Zr_2O_7$ + 2 $La_2O_3$ + 7 $O_2$ + 28 Li |

Table S8. Summary of DFT-predicted decomposition reactions related to the voltage stability window of $Li_6Zr_2O_7$ which is one of the decomposition phases of garnet-type $Li_7La_3Zr_2O_{12}$ (LLZO).

| Voltage / V vs. $Li/Li^+$ | Decomposition reaction |
|---|---|
| 0 – 0.04 | 2 $Li_6Zr_2O_7$ + 14 Li → $Zr_4O$ + 13 $Li_2O$ |
| 0.04 – 0.05 | 2 $Li_6Zr_2O_7$ + 13.33 Li → 1.333 $Zr_3O$ + 12.67 $Li_2O$ |
| 0.05 – 3.21 | 2 $Li_6Zr_2O_7$ → 2 $Li_6Zr_2O_7$ |
| 3.21 – 3.24 | 2 $Li_6Zr_2O_7$ → 4 $Li_2ZrO_3$ + $Li_2O_2$ + 2 Li |
| 3.24 – 3.39 | 2 $Li_6Zr_2O_7$ → 4 $Li_2ZrO_3$ + 0.25 $LiO_8$ + 3.75 Li |
| 3.39 – 3.72 | 2 $Li_6Zr_2O_7$ → 0.75 $LiO_8$ + 4 $ZrO_2$ + 11.25 Li |
| 3.72 – | 2 $Li_6Zr_2O_7$ → 4 $ZrO_2$ + 3 $O_2$ + 12 Li |

Table S9. Summary of DFT-predicted decomposition reactions related to the voltage stability window of $Li_2O$ which is one of the reductive decomposition phases of garnet-type $Li_7La_3Zr_2O_{12}$ (LLZO).

| Voltage / V vs. $Li/Li^+$ | Decomposition reaction |
|---|---|
| 0 – 2.90 | $Li_2O$ → $Li_2O$ |
| 2.90 – 3.24 | $Li_2O$ → 0.5 $Li_2O_2$ + Li |

| | |
|---|---|
| 3.24 – 3.72 | $Li_2O \rightarrow 0.125\ LiO_8 + 1.875\ Li$ |
| 3.72 – | $Li_2O \rightarrow 0.5\ O_2 + 2\ Li$ |

Table S10. Summary of DFT-predicted decomposition reactions related to the voltage stability window of $La_2O_3$ which is one of the reductive decomposition phases of garnet-type $Li_7La_3Zr_2O_{12}$ (LLZO).

| Voltage / V vs. $Li/Li^+$ | Decomposition reaction |
|---|---|
| 0 – | $La_2O_3 \rightarrow La_2O_3$ |

Table S11. Summary of DFT-predicted decomposition reactions related to the voltage stability window of garnet-type $Li_5La_3Ta_2O_{12}$ (LLTO).

| Voltage / V vs. $Li/Li^+$ | Decomposition reaction |
|---|---|
| 0 – 0.35 | $4\ Li_5La_3Ta_2O_{12} + 40\ Li \rightarrow 30\ Li_2O + 6\ La_2O_3 + 8\ Ta$ |
| 0.35 – 0.55 | $4\ Li_5La_3Ta_2O_{12} + 10\ Li \rightarrow 6\ Li_5TaO_5 + 6\ La_2O_3 + 2\ Ta$ |
| 0.55 – 0.65 | $4\ Li_5La_3Ta_2O_{12} + 2.5\ Li \rightarrow 7.5\ Li_3TaO_4 + 6\ La_2O_3 + 0.5\ Ta$ |
| 0.65 – 3.23 | $4\ Li_5La_3Ta_2O_{12} \rightarrow 6.667\ Li_3TaO_4 + 1.333\ La_3TaO_7 + 4\ La_2O_3$ |
| 3.23 – 3.24 | $4\ Li_5La_3Ta_2O_{12} \rightarrow 4\ La_3TaO_7 + 2\ Li_2O_2 + 4\ Li_3TaO_4 + 4\ Li$ |
| 3.24 – 3.47 | $4\ Li_5La_3Ta_2O_{12} \rightarrow 0.5\ LiO_8 + 4\ La_3TaO_7 + 4\ Li_3TaO_4 + 7.5\ Li$ |
| 3.47 – 3.72 | $4\ Li_5La_3Ta_2O_{12} \rightarrow 1.25\ LiO_8 + 2\ La_3TaO_7 + 6\ LaTaO_4 + 18.75\ Li$ |
| 3.72 – | $4\ Li_5La_3Ta_2O_{12} \rightarrow 2\ La_3TaO_7 + 6\ LaTaO_4 + 5\ O_2 + 20\ Li$ |

Table S12. Summary of DFT-predicted decomposition reactions related to the voltage stability window of $Li_3TaO_4$ which is one of the reductive decomposition phases of garnet-type $Li_5La_3Ta_2O_{12}$ (LLTO).

| Voltage / V vs. $Li/Li^+$ | Decomposition reaction |
|---|---|
| 0 – 0.35 | $Li_3TaO_4 + 5\ Li \rightarrow 4\ Li_2O + Ta$ |
| 0.35 – 0.55 | $Li_3TaO_4 + Li \rightarrow 0.8\ Li_5TaO_5 + 0.2\ Ta$ |
| 0.55 – 3.59 | $Li_3TaO_4 \rightarrow Li_3TaO_4$ |
| 3.59 – 3.72 | $Li_3TaO_4 \rightarrow LiTaO_3 + 0.125\ LiO_8 + 1.875\ Li$ |

| | |
|---|---|
| 3.72 – 3.94 | $Li_3TaO_4$ → $LiTaO_3$ + 0.5 $O_2$ + 2 Li |
| 3.94 – 4.03 | $Li_3TaO_4$ → 0.3333 $LiTa_3O_8$ + 0.6667 $O_2$ + 2.667 Li |
| 4.03 – | $Li_3TaO_4$ → 0.5 $Ta_2O_5$ + 0.75 $O_2$ + 3 Li |

Table S13. Summary of DFT-predicted decomposition reactions related to the voltage stability window of $Li_5TaO_5$ which is one of the reductive decomposition phases of $Li_3TaO_4$.

| Voltage / V vs. $Li/Li^+$ | Decomposition reaction |
|---|---|
| 0 – 0.35 | $Li_5TaO_5$ + 5 Li → 5 $Li_2O$ + Ta |
| 0.35 – 3.10 | $Li_5TaO_5$ → $Li_5TaO_5$ |
| 3.10 – 3.24 | $Li_5TaO_5$ → 0.5 $Li_2O_2$ + $Li_3TaO_4$ + Li |
| 3.24 – 3.59 | $Li_5TaO_5$ → $Li_3TaO_4$ + 0.125 $LiO_8$ + 1.875 Li |
| 3.59 – 3.72 | $Li_5TaO_5$ → $LiTaO_3$ + 0.25 $LiO_8$ + 3.75 Li |
| 3.72 – 3.94 | $Li_5TaO_5$ → $LiTaO_3$ + $O_2$ + 4 Li |
| 3.94 – 4.03 | $Li_5TaO_5$ → 0.3333 $LiTa_3O_8$ + 1.167 $O_2$ + 4.667 Li |
| 4.03 – | $Li_5TaO_5$ → 0.5 $Ta_2O_5$ + 1.25 $O_2$ + 5 Li |

Table S14. Summary of DFT-predicted decomposition reactions related to the voltage stability window of $La_3TaO_7$ which is one of the reductive decomposition phases of $Li_3TaO_4$.

| Voltage / V vs. $Li/Li^+$ | Decomposition reaction |
|---|---|
| 0 – 0.35 | $La_3TaO_7$ + 5 Li → 2.5 $Li_2O$ + 1.5 $La_2O_3$ + Ta |
| 0.35 – 0.55 | $La_3TaO_7$ + 2.5 Li → 0.5 $Li_5TaO_5$ + 1.5 $La_2O_3$ + 0.5 Ta |
| 0.55 – 0.65 | $La_3TaO_7$ + 1.875 Li → 0.625 $Li_3TaO_4$ + 1.5 $La_2O3$ + 0.375 Ta |
| 0.65 – | $La_3TaO_7$ → $La_3TaO_7$ |